Communications in Physics, Vol. 30, No. 3 (2020), pp. 279-299
DOI:10.15625/0868-3166/30/3/13858

MECHANISM OF INVERSE MAGNETORESISTANCE IN HIGH-T_a ANNEALED MnNi/Co/Ag(Cu)/Py SPIN VALVES

NGUYEN ANH TUAN[1,†], LUONG VAN SU[1,3], HOANG QUOC KHANH[1], TRAN THI HOAI DUNG[1] AND NGUYEN ANH TUE[2]

[1]*ITIMS, Hanoi Univ. of Science and Technology, 1 Dai Co Viet, Hai Ba Trung, Hanoi, Vietnam*

[2]*IEP, Hanoi Univ. of Science and Technology, 1 Dai Co Viet, Hai Ba Trung, Hanoi, Vietnam*

[3]*Faculty of Electrical and Electronic Engineering, Phenikaa Institute for Advanced Study (PIAS), Phenikaa University*

[†]*E-mail:* tuanna@itims.edu.vn

Received 5 June 2019

Accepted for publication 3 July 2020

Published 22 July 2020

Abstract. *The magnetic transport properties – magnetoresistive (MR) effects of MnNi/Co/Ag(Cu)/Py pinned spin valve structures (SVs) prepared by rf sputtering method and annealed at T_a = 100˚C - 500˚C for 30 minutes in high vacuum ($\sim 10^{-5}$ torr) are investigated. The received results show a change in the observed MR behaviors from a normal giant magnetoresistance effect to an inverse magnetoresistance effect after annealing at high temperatures, 300˚C and 400˚C, for these SVs. The origin and mechanism of the IMR behavior are analyzed and discussed. These results will suggest an ability to manufacture SV devices used the IMR effect for enhancing the application capacities for SV-sensor systems.*

Keywords: spin valve, magnetic transport, spin-dependent scattering, magnetoresistance (MR), inverse magnetoresistance (IMR).

Classification numbers: 73.21.Ac, 73.40.-c, 73.50.Jt, 73.63.Rt, 75.47.De, 75.70.Cn, 75.76.+j.

I. INTRODUCTION

Basically, a spin valve (SV) structure as presented in Fig. 1(a) is denoted as AFM/FM_2/NM/FM_1, where FM_1 and FM_2 are ferromagnetic (FM) layer separated from each other by a nonmagnetic (NM) layer (spacer), and AFM is an antiferromagnetic (AFM) layer. Notice that such structure consists of a trilayer FM_2/NM/FM_1 being attached to an AFM layer to form an SV element. Where $FM_1$is as a free FM layer with its M_1 magnetization can easily change its direction with a low magnetic field H, and the FM_2 layer is pinned for its M_2 magnetization by the AFM layer. The pinning is performed through an interlayer exchange coupling (IEC) between the AFM and FM_2 bilayers. These SVs are used to control the flow of the spin currents through an intervention of an external magnetic field by a well-known effect – giant magnetoresistance (GMR) effect, whose mechanism is thought to be by a spin-dependent scattering (SDS) [1,2]. It is also called the "spin valve" effect because the spin-polarized current is "opened" (low resistance) or "blocked" for a spin transportation. The spin currents are determined by the alignment of the M_1 and M_2 vectors in the "valve" between parallel or antiparallel configurations (Fig. 1(b)). The largest spin current (corresponding with the lowest resistance) can be achieved when the magnetizations are completely parallel at a high enough field $(H) : H > H_S$ (saturation field). The smallest one (highest resistance) is achieved once they are completely aligned antiparallel at low enough or zero fields, $H = 0$. The SV elements have been used widely in modern magnetic and electronic devices of the next generation devices – spintronics [3–6].

The normal GMR effect presents a negative variation of the electric resistance for the magnetic field intensity change. However, in some cases, the SV structures show an inverse behavior of the GMR effect indicated by a positive variation of the electric resistance: The resistance of the SV increases along with the rising intensity of H and reaches a maximum level once the M directions in two FM layers become fully parallel when $H \geq H_S$; and vice versa, the resistance reaches a minimum level when these directions become antiparallel at $H = 0$ (Fig. 1(c)). In these cases, the GMR effect is called *the inverse magnetoresistance* (IMR). The IMR effect has been observed in the magnetic multi-layer systems with various types of structures [7–17]. The mechanism by which the IMR effect is caused in these structures was primarily based on modulating the

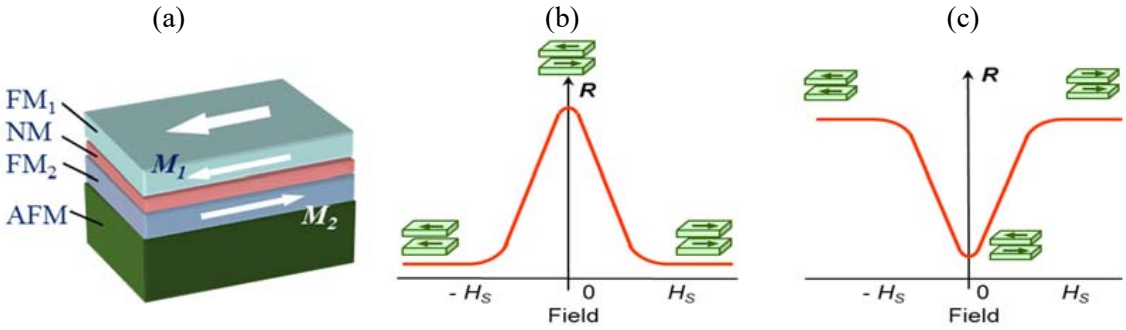

Fig. 1. (a) Principal schema of a basic spin-valve structure. (b) Normal GMR effect indicates a negative MR behavior. (c) Inverse GMR effect, or IMR effect, indicates a positive MR behavior.

spin-dependent conductivity of one of the two FM layers, hence, inverting the spin state density (SSD) at the Fermi level in that FM layer [7–13].

So far, the GMR effect has been apprehended thoroughly and the SV structures have been comprehensively reported. However, specific technical status in the manufacture that gives rise to new effects is still useful for adjusting, modifying, or applying to technology processes, because the performance of GMR is extremely sensitive to fabricated conditions [17]. Two SV systems with two different NM spacer layers: Ag and Cu corresponded with the MnNi/Co/Ag/Py and MnNi/Co/Cu/Py SV structures (see Fig. 2(a)) have been chosen to be investigated. By using the rather thick Ag and Cu layers, such as 6 nm and 12 nm, and the difference in coercivities of the two Py and Co layers, a non-coupled (or very weak-coupled) sandwich-type SV structure is mentioned in this study. For such SV structures, interlayer magnetic coupling is not a necessary condition, and magnetic structural changes made by any reason may also cause an MR effect. The applicability of these SV structures, which here focuses on the MR effect appearing even in very weak magnetic fields, is the most important thing [18]. Even though, as expected, the normal GMR effects were observed for the samples annealed at medium temperatures (T_a), usually $T_a < 300^{\circ}$C, it is not the highlight of this study. It is worth noting that, out of expectation, the IMR effect has been observed for samples annealed at high temperatures, usually at $T_a \geq 300^{\circ}$C. Therefore, this paper focuses only on the physical origin of the mechanism that causes the IMR effect in this SVs. Learning from these results will suggest an applicability to combine two types of SV with GMR and IMR effects in the same component to create new capabilities for spintronics applications.

II. EXPERIMENT

The samples of the MnNi/Co/Ag(Cu)/Py SVs (Fig. 2(a)), in which MnNi and Py (permalloy) were $Mn_{50}Ni_{50}$ and $Ni_{81}Fe_{19}$alloys, respectively, were fabricated by using *rf* sputtering technique with an *rf* sputtering power of 300 W, to be deposited on the Si(100)/SiO_2 substrates. The base vacuum was lower than $\sim 10^{-6}$ mbar and the sputtering pressure of argon was $\sim 10^{-3}$ mbar. In this study, the MnNi-alloy, Py-alloy, Co, Ag, and Cu 3-inch targets were used, with the distance between the target and the substrate was approximately 8 cm. The deposition parameters, such as the ratio R, which was determined to experimentally correspond with each layer through measurements of the thicknesses (Alpha-step IQ from KLAT-Tencor corporation) that were deposited for a given time, were $R_{MnNi} \sim 3$ nm/min; $R_{Co} \sim 1.7$ nm/min; $R_{Py} \sim 1.8$ nm/min; $R_{Ag} \sim 7.2$ nm/min, and $R_{Cu} \sim 3.5$ nm/min. Thus, nominal thicknesses corresponding with each layer were determined to be $t_{MnNi} = 25$ nm, $t_{Co} = t_{Py} = 15$ nm, t_{Ag} (and also t_{Cu}) $= 6$ nm and 12 nm by the deposition rate R and time of deposition duration for each layer. A Si mask with rectangular slits (width of 1 mm and length of 10 mm) was used to shape the samples into a rectangular-bar form with the size of 1×10 mm^2 (Fig. 2(b)). These samples then were treated by post-deposited annealing at various temperatures (T_a) of 100˚C, 200˚C, 300˚C, and 400˚C (most of the magnetic properties of the samples dissolved after annealed at 500˚C) in the base vacuum of $\sim 10^{-5}$ mbar for 0.5 hours before investigating the magnetic properties and the transport properties.

Magnetic properties of the SV samples were investigated through the magnetization measurements using a DMS 880 vibrating sample magnetometer (VSM) by Digital Measurements System Inc., with the magnetic field parallels the film plane and were directed along the long axis of the sample bar – sample-axis (Fig. 2(c)). GMR effect was measured using a standard *dc* four-point probe method under a *dc* magnetic field $\boldsymbol{H}$ being maintained and controlled by the VSM with

a super-stable *dc* current of 10 mA. The field $\boldsymbol{H}$ is applied in the sample plane and parallels the sample-axis direction in the so-called current-in-plane (CIP) geometry for current density $\boldsymbol{j}$ (see Fig.2(c)) with scanning step of 2 Oe. Some MR measurements in an in-plane transversal H configuration to test the AMR effect have also been implemented. Nevertheless, the received results have confirmed that there is no AMR effect in these SV systems. All measurements were conducted. GMR ratio is defined by GMR = ΔR/R(0) = $\{$[R(H) – R(0)]/R(0)$\}\times 100$ (%), where R(H) and R(0) are the sample resistances being measured at a magnetic field H and at H = 0, respectively.

III. RESULTS AND DISCUSSION

As mentioned above, all the MnNi/Co/Ag(Cu)/Py SV samples, after being deposited and post-annealed at various T_a's, have been investigated the magnetic properties and MR features, but are not presented here due to normal features in magnetic properties and GMR behaviors of these SV systems when $T_a < 300^{\circ}$C. However, for more complete presentation, Fig. 3 shows selected results of both magnetic properties and GMR annealed at below 300°C in some cases. The results for the case of $T_a < 300^{\circ}$C are not analyzed in detail here. Nonetheless, they have given information on the behaviors of magnetic coupling and magnetic structural changes between Py and Co layers depending on the thickness of the NM spacer layers (t_{Ag} and t_{Cu}) and annealing temperature T_a. A pinned phenomenon of the Co layer arranged adjacent to the MnNi layer, as well as the normal GMR effect of both SV samples, have also been illustrated by those results. For the case of $T_a \geq 300^{\circ}$C, a more detailed analysis of magnetic properties and magnetic coupling had been presented in our other work [19]. Generally, in all the samples, magnetic properties as a function of t_{Ag}, t_{Cu} and T_a show some common features often received in SV-type systems. For example, thickness- and annealing-dependent properties in the magnetic coupling between the FM layers express an oscillatory-like behaviors between FM-type and AFM-type arrangement, or changes in the coercive force H_C. Both the manifestations have ever been observed in multilayers [1, 20–23], or SV and trilayer structures [24–26]. A study on Co/Ag multilayer films has suggested the role of annealing on the magnetic properties of the SVs, which relevant directly to the Co/Ag(Cu) or Py/Ag(Cu) interfaces [26]. It has been pointed out that the interface roughness, associated to a "back-diffusion" process in the Co/Ag interfaces, is most crucial for the determination of the strength of the magnetic coupling between adjacent FM layers, transport properties, and also of the behavior of the coercivity and/or interface anisotropy. Some salient points in the magnetic properties of these SVs with quite thick thicknesses of t_{Ag} and $t_{Cu} = 6$ and 12 nm received from Ref. [19] can be summarized as follows.

(i) A non-coupled or an extremely weak-coupled behavior implied a rather random orientation of the magnetizations in the Py and Co layers for these SV systems. A two-step feature of the $M(H)$ loops, as seen in some cases in Figs. 3 (a), (b), indicates just an immensely weak interlayer coupling that is negligible in these SVs [18], and it comes from different H_C between Co and Py. Although presenting a non-coupled or very weak-coupled behavior, the in-plane $M(H)$ loops of the two SV systems still indicate a dominant tendency in a weak AFM-type coupling rather than strong AFM-type or FM-type coupling (Fig. 4(a) and (b)). Depending on t_{Ag}, $t_{Cu}$and T_a, leaf-shape loops that tend to be more upright can represent a FM-type coupling. Besides that, the SVs seem also to indicate a common tendency of out-of-plane anisotropy.

(ii) These SV systems have a tendency of an out-of-plane anisotropy whose origin is mainly attributed to a certain out-of-plane anisotropy induced by some interactions within the entire SV

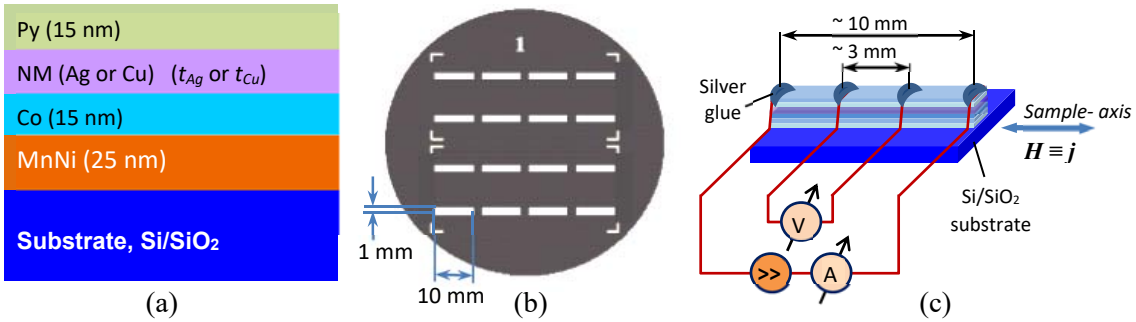

Fig. 2. (a) Schematic in cross-section of the MnNi/Co/Ag(Cu)/Py SV samples, with thicknesses corresponding with each layer are indicated. (b) Si mask with slits of 1 mm width and 10 mm length. (c) Experimental setup for GMR measurements of a standard *dc* four-point probe method in a CIP-configuration interrelated parallels between magnetic field $\boldsymbol{H}$ and current $\boldsymbol{j}$.

structure. It has been known that an ultrathin Co layer usually may have a perpendicular anisotropy originated basically from magnetic surface anisotropy [27–29]. The induction of this magnetic anisotropy will be discussed in more detail below. However, as illustrated in Fig. 4(a), a demagnetization field H_d induced significantly by the bar-form samples can considerably diminish this out-of-plane anisotropy. Therefore, in fact, the altitude angle, β, is considered as very small and $\boldsymbol{M}_2\text{'} \equiv \boldsymbol{M}_2$. This explains why the $M(H)$ loops of the SVs showed a quite faint FM-type alignment, which presents a non-coupled or very weak-coupled behavior, as mentioned above. A cusp-like magnetization curve, as shown in Fig. 3(a), (b), may be created due to the presence of competing first and second order uniaxial anisotropy components [30].

(*iii*) By comparing different materials being used for the NM layers (Ag and Cu), it is noticed that a FM-type feature is more dominant in the MnNi/Co/Ag/Py SVs rather than in the MnNi/Co/Cu/Py SVs that show a clearer tendency of an AFM-type feature with a more typical leaf-shape style of the loops, especially for the sample annealed at high-T_a's. Moreover, an effective H_C enhanced quite clearly when utilizing Cu as the spacer layer in the SVs, (compare Fig. 3(a) and (b), and see Ref. [19]).

(*iv*) An enhanced H_C coercive force through coupling to the AFM NiMn layer because of the exchange anisotropy between MnNi and Co layers was received. This provides evidence of some changes in the magnetization alignment between the FM- and AFM-types of the Py and Co layers depending on the t_{Ag} and t_{Cu} thicknesses. The leaf-shape tendency with a slight gentler slope of virgin magnetization curves of the loops which indicated a more prominent AFM-type alignment is more dominant in the SVs with thinner-t_{Ag}'s and -t_{Cu}'s (t_{Ag} and t_{Cu} = 6 nm) than those in the SVs with thicker-t_{Ag}'s and -t_{Cu}'s (t_{Ag} and t_{Cu} = 12 nm).

(*v*) Generally, for the SVs annealed at different high-T_a's, magnetic properties indicate a more prominent FM-type alignment for the SVs annealed at 400˚C than at 300˚C, in both the cases of t_{Ag}, t_{Cu} = 6 nm and t_{Ag}, t_{Cu} = 12 nm. This result for annealing at high-T_a's is also consistent with a similar conclusion recently made when studying on the interlayer exchange coupling in trilayer structures [31]. This indicates a more perpendicular tendency of the SVs annealed at 400˚C.

Another effect of the annealing process (T_a) on magnetic properties is a substantial enhancement of the H_C coercivity for the samples annealed at the high-T_a's. This is a consequence of the magnetocrystalline anisotropy characterized by a total effective K_u/M_S ratio of the SVs and the so-called exchange-bias coupling (EBC) between the MnNi and Co layers. An exchange-biased field H_{ex} that characterized by this coupling will be mentioned below.

(vi) The impact of the positive EBC phenomenon induced by the MnNi/Co interfaces has been observed for both the SV systems. However, the exchange-biased fields H_{ex} received in these SV systems were only several oersteds, $H_{ex} \sim +2 \div 5$ Oe, and had a positive shift tendency as analyzed in detail by Ref. [19]. Firstly, the weak in-plane exchange bias fields are since the SVs were not cool down in a magnetic field after annealing as we expected to obtain the exchange bias and control the H_{ex} without a cooling field as suggested in Refs. [32, 33]. This has opened some proficiencies and opportunities to tune the exchange bias even after device fabrication [32]. Secondly, this phenomenon could be the result of a high-temperature annealing process that caused a deviation in a chemical stoichiometry of the MnNi AFM alloy, as well as a collapse of the MnNi/Co interfaces. It has been confirmed that high annealing temperature leads to inter-diffusion and decrease H_{ex} [34].

Positive EBC behaviors have been observed in many FM/AFM bilayer systems when an applied external magnetic field is directed out of the anisotropic axis or the sample plane as pointed out in some studies [35–38]. However, in this study, the external field was applied along the easy axis of the sample (see Fig. 4(a)). In other words, either the anisotropic axis of the samples or the orientation of the EBC between FM and AFM domains tended to slightly orient out of the sample plane (e.g. see Fig. 4(c)). For a better understand of this phenomenon, we should distinguish between the EBC and magnetic interlayer exchange coupling (IEC). For the EBC, it is an interaction only between the two FM and AFM layers having direct contact, which is an exchange anisotropy coupling, and furthermore an interfacial unidirectional anisotropy [39]. For a contact system of a FM/AFM bilayer, an effective bias field H_{eb}, on the FM thin film was produced by the interfacial exchange with the AFM film. The EBC energy mentioned here is an interfacial unidirectional energy density and is determined by $E_{eb} = t_{FM}M_S H_{eb}$, with M_S and t_{FM} being the saturation magnetization and thickness of the FM layer, respectively. In this case, H_{eb} which was determined by the uncompensated AFM interfacial spin density [39] is completely different from H_{ex} as assigned to the whole pinning SV system. In this situation, lower anisotropy energies of the AFM layer increaseH_C of the FM layer. Regarding the EBC between FM and AFM layers for a whole system of spin valve type AFM/FM_2/NM/FM_1, with the presence of random unidirectional anisotropy field at the AF interface, the influence of FM/AFM interface structure, especially the role of the interface roughness due to randomness on the hysteresis mechanism and EBC behavior for this SV system has been recently pointed out by the Yüksel's model [40]. Hamiltonian introduced in this model takes into account many different exchange interactions. These interactions include the coupling between the nearest neighbor spin couples, in which takes the spin couples located in free as well as pinned FM layers, the AFM exchange coupling between AFM spins, the exchange coupling at the interface region where pinned FM spins interact with AFM spins, and also set an easy axis for the magnetization direction for both the FM and AFM layers. This model demonstrated that with a rough interface structure at the FM/AFM interface region, uncompensated AFM interface spins (see Fig. 4(c)) may be originated. These spins can be responsible for the origination of a non-zeroH_{ex} field. Another conclusion is that an exchange anisotropy induced

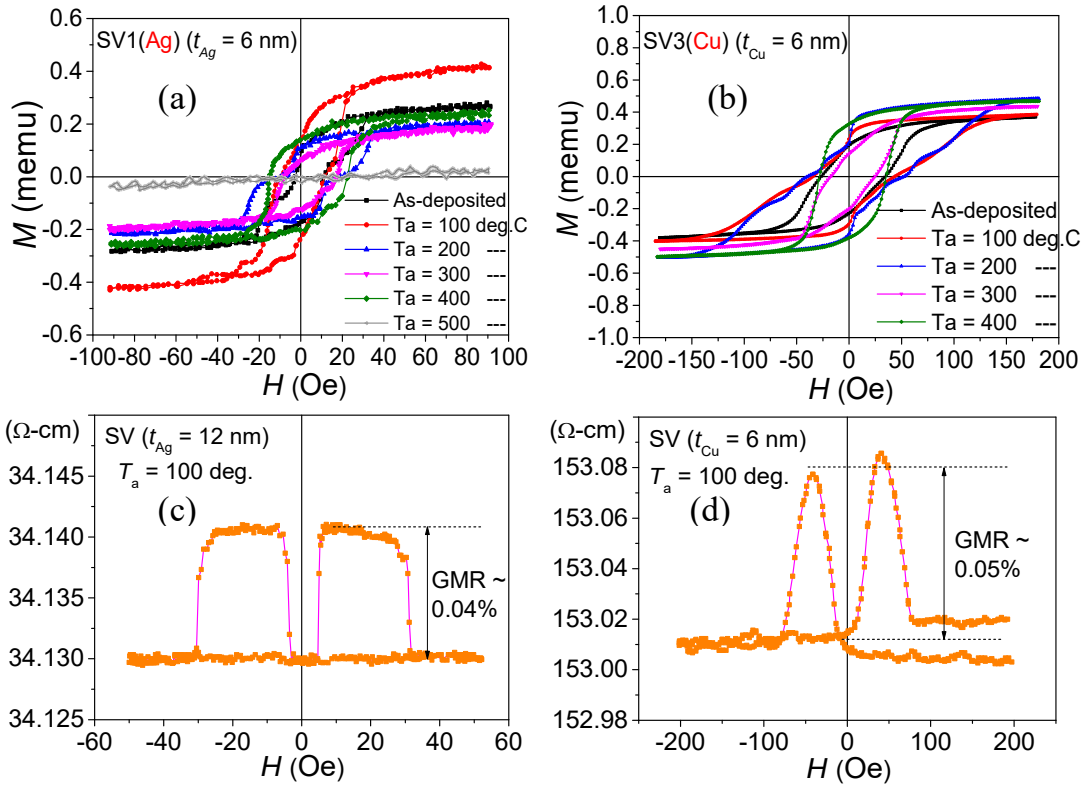

Fig. 3. (a)-(b) $M(H)$ loops of the MnNi/Co/Ag(Cu)/Py samples (with $t_{Ag} = t_{Cu} = 6$ nm) as deposited and annealed from T_a= 100˚C to 400˚C for 30 mins. The SV1 sample annealed at T_a= 500˚C presents a collapsed magnetic properties. (c)-(d) Normal GMR effects observed in the SV samples with t_{Ag} = 12 nm and t_{Cu} = 6 nm annealed at T_a = 100˚C.

uniformly at the FM/AFM interface causes a significant shift of the M(H) loop along the field axis, and the H_{ex} increases with increasing amount of disorder and gradually reduces towards zero with further increasing randomness. Different forms of the FM/AFM interface roughness due to the randomness of anisotropy field may lead to different behavior of exchange bias. As a result, this suggests that the in-plane unidirectional anisotropy constant $J_K \equiv M_s d_{Co} H_{ex}$ of the SV system MnNi/Co/Ag(Cu)/Py, where M_s and d_{Co} are saturation magnetization and thickness of the Co layer respectively, is small due to the moderately weak H_{ex}.

On the other hand, some other studies suggested that apart from the perpendicular anisotropy, the positive-shift effect of the $M(H)$ loops can also be produced by the thicker-AFM thickness [41]. As in this study with d_{NiMn} of the MnNi layer up to 25 nm, the IEC can be induced by EBC field from the perpendicular anisotropy between the Co layer and the MnNi layer. This also implies an important suggestion for the perpendicular EBC applications in the SVs. From the results analyzed above, it is a hint that perpendicular-type morphology in the spin exchange coupling at the Co/MnNi interfaces is a realistic possibility. Moreover, the bending to create two-step-like features observed in some $M(H)$ loops as seen rather clearly in Figs. 3 and 4 can also

indicate a contribution of the so-called double-shifted phenomenon in the hysteresis loops. This is also a real possibility because the double-shifted effect usually occurs when the FM/AFM system is either zero-field cooled in a demagnetized state, or grown in zero-field due to an imprint of the domain pattern of the FM into the AFM during the post-annealing cooling procedure [42]. The technique of growing in the zero-field for the SV samples was also performed in this study. Consequently, a distribution in blocking temperature $T_B$of the SV system which origins from the distribution of grain-sizes, stoichiometry, strains, or defects in the layers can be achieved [42, 43]. The outstanding features in magnetic properties above suggested a tilted-type granular structure of the Co/MnNi bilayer in these SV systems as illustrated in Fig. 4(c).

Meanwhile, IEC is a magnetostatic coupling between two FM layers separated by a nonmagnetic (NM) layer (such as Co/Ag(Cu)/Py sandwich), which is a bilinear coupling, and in the most general sense, follows an RKKY-like interacting mechanism [44]. In this case, the IEC energy specifies a coercivity of this "sandwich" system. Thus, the coercivity H_C of the whole pinning SV system must be a right combination of H_C of the single FM layer contacting with the AFM layer and the coercivity of that "sandwich" system. Therefore, the consequence of the total magnetic interaction in the pinning SV structure MnNi/Co/Ag(Cu)/Py that was received in this study with the hysteresis loop curves, as shown above, is an effective combination, at least of both the EBC and IEC couplings. It is possible to imagine an effective interaction derived from the two main types of interactions in the SV structure MnNi/Co/Ag(Cu)/Py as follows (regarding to Fig. 4). The EBC between the MnNi and the Co layers, without the IEC between the Co and Py layers, results in the pinning of the magnetization $\boldsymbol{M}_2$ of the Co layer. Meanwhile, the IEC between the Co layer and the Py layer (with its magnetization is the $\boldsymbol{M}_1$), in which the Co layer is not pinned by the MnNi layer due to the EBC mechanism, follows the so-called RKKY mechanism through the Ag(Cu) spacers. In addition to those, there are other important interactions. For

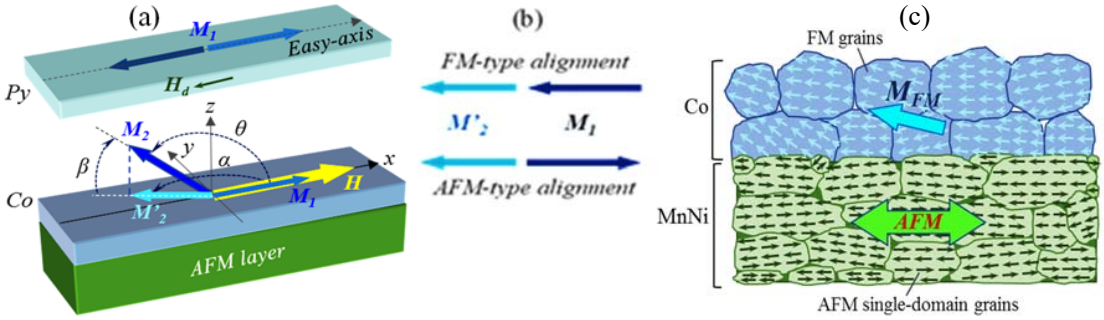

Fig. 4. (a) Geometric performances of magnetic behaviors of the Py and Co layers, in which the $\boldsymbol{M}_1$ magnetization of the Py layer is supposed to lie along easy-axis of the sample bar; and the $\boldsymbol{M}_2$ magnetization of the Co layer is assumed to direct out-of-plane by an altitude of β with its in-plane $\boldsymbol{M'}_2$ component creates an azimuth of α. (b) Representation of the FM- and AFM-type alignments for $\boldsymbol{M}_1$ and $\boldsymbol{M'}_2$ components of the SVs (with the case of the $\beta = 0$ and $\alpha = 180^\circ$). (c) Depiction of a tilted-type grain morphology (out-of-plane anisotropic) in the Co layer and a multi-domain (or grain-type) structure in the MnNi layer. (After Ref. [19]).

example, consideration should be given to interacting with the demagnetization field $\boldsymbol{H}_d$ which is an in-plane field formed by some surface roughness (it is a "dipolar surface anisotropy") [27], and with the magnetocrystalline anisotropic field $\boldsymbol{H}_K$. The IEC energy E_{int} can be determined as $E_{int} = -j_1[\boldsymbol{M}_1\boldsymbol{M}_2/(|M_1||M_2|)] - j_1[\boldsymbol{M}_1\boldsymbol{M}_2/(|M_1||M_2|)]^2 = -j_1\cos(\theta) - j_2\cos^2(\theta)$, where θ is the angle between the magnetization vectors of the FM layers [45] (see Fig. 4(a)). The first term with the parameter j_1 representing the bilinear coupling describes the parallel (P) and antiparallel (AP) alignment of the magnetizations corresponding with $\theta = 0^\circ$ and 180°. The second term with j_2 describes the biquadratic coupling corresponding with $\theta = 90^\circ$. In the case of the slightly weak out-of-plane anisotropy (with $\beta \sim 0$ and $\alpha \sim 0$ or $\sim 180^\circ$) $\boldsymbol{M}_2$ is replaced by $\boldsymbol{M}_2$**'**, and a geometrical configuration as in Fig. 4(b) is used. Therefore, j_2 of biquadratic coupling can be neglected, and $E_{int} \approx -j_1\cos(\alpha) \approx -j_1 = j/(2A)$, where j is the IEC constant per interface area A determined by the difference in energy between parallel and antiparallel configurations: $j = (E_{anti} - E_{par})/(2A)$ [39]. Note that the IEC is extremely weak as recorded in the SV systems due to $t_{Ag(Cu)}$ is rather thick leading to j is also very small. Depending on the NM thickness, j can be positive or negative, so that the coupling is ferromagnetic or antiferromagnetic types which favor $\boldsymbol{M}_1$ and $\boldsymbol{M}_2$ (or $\boldsymbol{M}_2$**'**) magnetizations in P or AP configurations, respectively. Many studies are aware of this phenomenon [8, 24, 46]. Regarding the bilinear coupling constant $J$of a trilayer FM_1/NM/FM_2 with a noble-metal spacer NM, J as a function of Ag thickness also demonstrates an oscillation with two short and long periods [24]. A recent study on the interlayer exchange coupling in trilayer structures took into consideration both bi-linear (j_1, corresponding to $\theta = 0^\circ$) and bi-quadratic (j_2, corresponding to $\theta = 90^\circ$) coupling components [31]. It has indicated that the sign of j_1–$2j_2$ determines whether the coupling is FM- or AFM-type. If $j_1 > 0$ and $j_1 \geq 2j_2$, then the coupling is FM; if $|j_1| < 2j_2$, then the coupling is non-collinear, and if $j_1 < 0$ and $|j_1| \geq 2j_2$, then the coupling is AFM. This suggests a possibility of further analysis and evaluation of the factor that generates the out-of-plane anisotropy for the coupling between the $\boldsymbol{M}_1$ and $\boldsymbol{M}_2$, by the j_2 component.

After summarizing the analysis from the magnetic interactions mentioned above, it can be conjectured that the origin of the out-of-plane anisotropy observed in the SV structures may come from the certain random distribution of the interface magnetic anisotropy. As a result, slightly out-of-plane tendency of spins in the AFM domains at the FM/AFM junction has been established so that an effective magnetic anisotropic field induces an overall magnetic anisotropy in the entire SV systems. Perhaps, that can explain why there is a manifestation of the out-of-plane anisotropy for the SV systems studied here. In this study, there is a possibility of a significant positive shift in the hysteresis loops, with the effect of the out-of-plane anisotropy then the total shift which is an effective result due to the competition between positive EBC and the out-of-plane anisotropy that will tend to shift less towards the positive. Therefore, H_{ex} is small. Thus, the weak H_{ex} and positive exchange-bias behaviors once again proved that there was some tendency for an overall effective magnetic anisotropy in these SV systems to direct out-of-plane, as illustrated geometrically in Fig. 4(a) for the $\boldsymbol{M}_2$ magnetization of the Co layers with $\alpha > 90^\circ$. Nonetheless, a more elaborate study of the out-of-plane magnetic anisotropy of the MnNi interface here should be also conducted since out-of-plane AF spin components are necessary to obtain out-of-plane exchange coupling [47].

Going back to the main analysis for the results presented in this study is about the IMR behaviors in $MR(H)$ curves of the weak-coupled MnNi/Co/Ag(Cu)/Py SVs annealed at high-T_a's

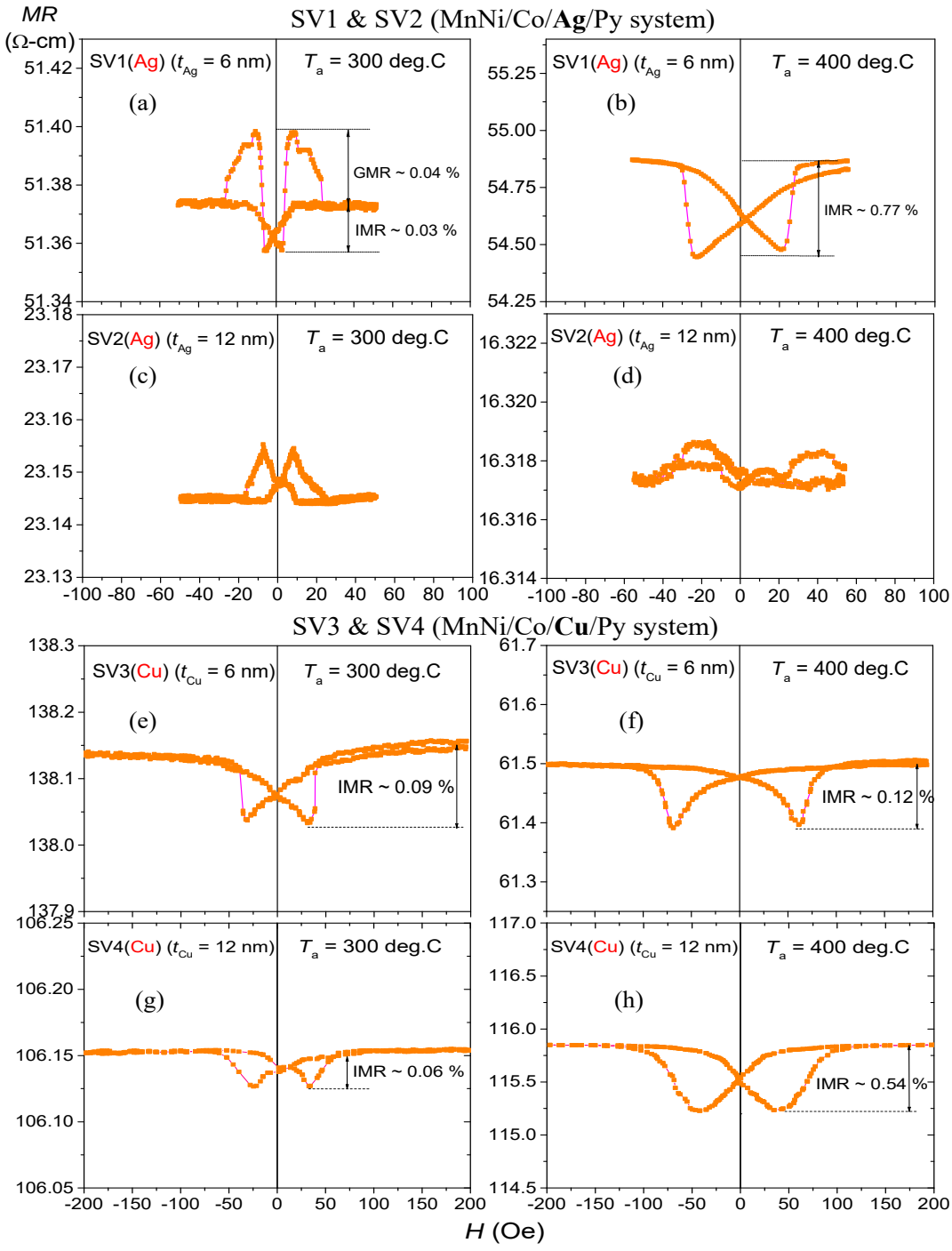

Fig. 5. $MR(H)$ curves of the samples annealed at T_a= 300˚C and 400˚C for 30 mins corresponding to: (a)-(d) the MnNi/Co/Ag(t_{Ag})/Py system with t_{Ag} = 6 nm (SV1) and 12 nm (SV2); and (e)-(h) the MnNi/Co/Cu(t_{Cu})/Py system with t_{Cu} = 6 nm (SV3) and 12 nm (SV4).

of 300˚C and 400˚C for 30 minutes. Fig. 5 shows the $MR(H)$ curves of the SVs with t_{Ag} and t_{Cu} = 6 nm and 12 nm, which are denoted by SV1-SV4, respectively. As seen in Fig. 5(a)-(d) for the SV1-SV2 of the MnNi/Co/Ag/Py system used the NM layer being Ag, in general, the IMR behaviors dominantly express just in the low-field region of about ±10 Oe around the zero origin with an IMR ratio of roughly 0.03 % for SV1 ($t_{Ag} = 6$ nm) annealed at 300˚C and a lower percentage for SV2 ($t_{Ag} = 12$ nm) annealed at 400˚C. Meanwhile, this system still mainly shows the normal GMR effects, for example, with an MR ratio of approximately 0.04% in the higher field region around ±15-25 Oe for SV1 annealed at 300˚C, and around ±20 Oe for SV2 annealed at both 300˚C and 400˚C. The SV1 annealed at 400˚C shows only the pure IMR effect with a maximum IMR ratio of about 0.77% (Fig. 5(b)). Whereas the MnNi/Co/Cu/Py SV system used the NM layer being Cu, SV3-SV4 seem to express only the pure IMR effect as shown in Fig. 5(e)-(h). Therefore, for the weak-coupled SV systems annealed at high-Ta's, the IMR effect seems to become stronger (see maximum IMR ratio) and more obvious when the NM layer is Cu and t_{Ag} and t_{Cu} turns thicker (12 nm) and T_a is higher (400˚C).

The early origin of the IMR can be found in some first publications [7, 8]. The general idea of the physical mechanism for the IMR can be described shortly as follows. In the framework of the Mott's two-current model for conduction in ferromagnets [48, 49], each FM layer in the SV structures, the Co and Py layers, has an own spin-dependent resistivity (SDR), $\rho^{\downarrow}_{Co(Py)}$ and $\rho^{\uparrow}_{Co(Py)}$ corresponding with the majority spin ($^{\downarrow}$) and minority spin ($^{\uparrow}$) channels of Co or Py. It is the difference in scattering probability $D^{\downarrow(\uparrow)}$ in each the spin channel: $D^{\downarrow} \neq D^{\uparrow}$ [8] that causes $\rho^{\downarrow}_{Co(Py)} \neq \rho^{\uparrow}_{Co(Py)}$ [49]. Therefore, a parameter of spin scattering asymmetry (SSA) between these channels, which is determined as the ratio of $\alpha_{Co(Py)} = \rho^{\downarrow}_{Co(Py)}/\rho^{\uparrow}_{Co(Py)} = D^{\downarrow}/D^{\uparrow}$, has been introduced [7, 8, 49]. Because of $D^{\downarrow(\uparrow)} \sim N^{\downarrow(\uparrow)}(E_F)$ where $N^{\downarrow(\uparrow)}(E_F)$ is the density of state (DOS) at the Fermi energy of the corresponding spin channels, $\alpha_{Co(Py)} = N^{\downarrow}(E_F)/N^{\uparrow}(E_F)$. In the context of spin-dependent (SD) conductivity (SDC) $\sigma^{\downarrow(\uparrow)}$ in a ferromagnet, because $1/\rho^{\downarrow(\uparrow)} = \sigma^{\downarrow(\uparrow)}$, the SSA parameter α can be represented as the ratio of the SDCs: $\alpha_{Co(Py)} = \sigma^{\uparrow}_{Co(Py)}/\sigma^{\downarrow}_{Co(Py)}$. For Co and Py, it has been confirmed that, normally, $N^{\downarrow}_{Co(Py)}(E_F) > N^{\uparrow}_{Co(Py)}(E_F)$ [50, 51] as sketched and indicated in Fig. 6(a). It is clear that normal MR effects occur when the parameter α is the same characteristic in the both Co and Py layers, either $\alpha_{\mathrm{Co(Py)}} > 1$ or $\alpha_{\mathrm{Co(Py)}} < 1$ [7].

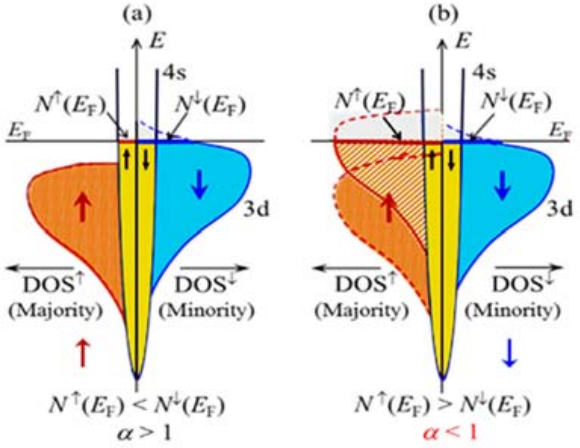

Fig. 6. Schematic illustration of 4s-3d band structures for density of states (DOS) in the FM layers with the correlation between DOS$^{\uparrow(\downarrow)}(E)$ at the Fermi energy, $N^{\uparrow(\downarrow)}(E_F)$, concerned to the case of (a) $N^{\downarrow}(E_F) > N^{\uparrow}(E_F)$ corresponding with $\alpha > 1$, and (b) $N^{\downarrow}(E_F) < N^{\uparrow}(E_F)$ leading to $\alpha < 1$.

The IMR effect occurs if only one of the FM layers has $\alpha_{\mathrm{Co(Py)}} < 1$, the other is still $\alpha_{(Co)Py} > 1$ [8]. Fig. 6(a,b) represents a 3*d*-band schematic of the FM layers for the case of $\alpha > 1$ and $\alpha < 1$, respectively. In order to inverse the DOS of a majority or minority 3d-spin band so that a certain $N^{\uparrow(\downarrow)}(E)$ is shifted to lead to an inversion of the SSA parameter from $\alpha > 1$ to $\alpha < 1$, as illustrated in Fig. 6(b), it is possible to use many different ways as mentioned in Ref. [46]. One of these ways is alloying of one of two FM layers, as firstly performed by Renard *et al*. [8]. The alloying leads to an addition of 3*d* majority spins to increase the $N^{\uparrow}(E)$ band, whereas the $N^{\downarrow}(E)$ band is still essentially unchanged. As a result, this caused the expected conversion: $N^{\downarrow}(E_F) < N^{\uparrow}(E_F)$, or $\alpha < 1$, as depicted in Fig. 6(b) (the dotted curve on left branch of this figure depicts the old corresponded to the left branch in Fig. 6(a)).

Figure 7 presents a simple schema in two different demonstrations for the mechanism of the normal GMR effect: SD scattering schema in each layer (Fig. 7(a,b)), with AP and P configurations for ***M*** corresponding to 4*s*-3*d* band structures in each layer, are indicated], and inter-band spin-transport schema based on FM band structures for DOS features of Co and Py (Fig. 7(c,d)).

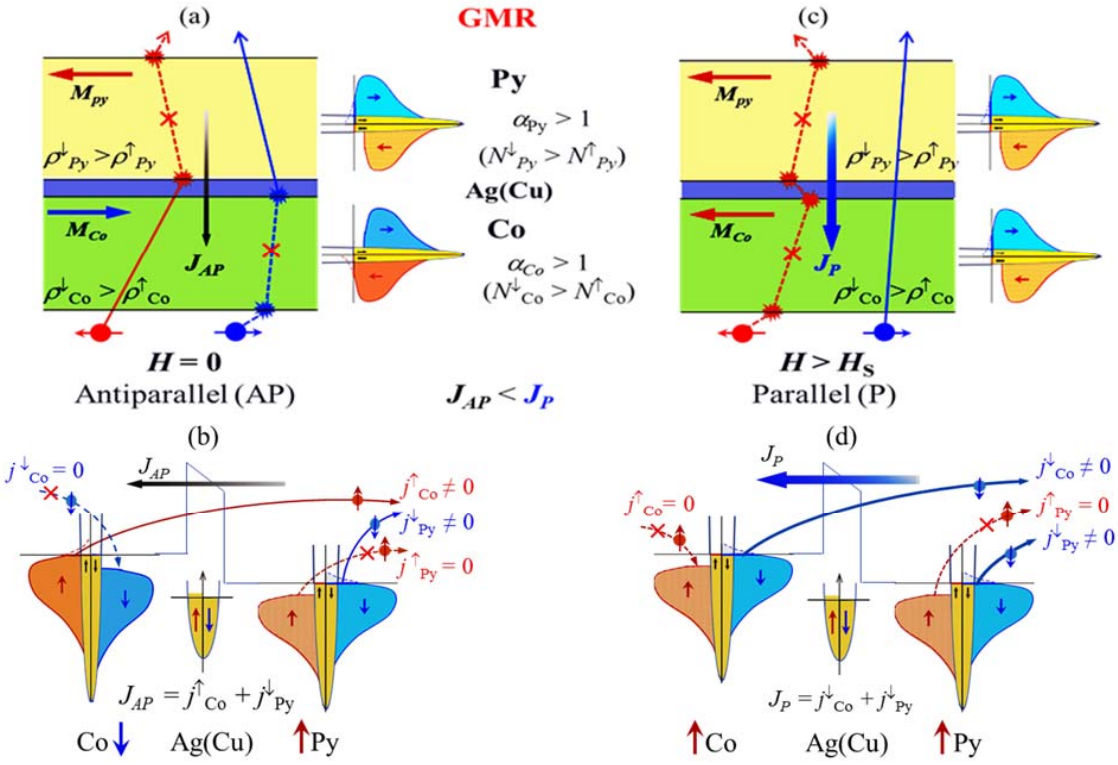

Fig. 7. Mechanism of the SD scattering for appearance of normal GMR effect in the low-T_a annealed SVs: (a) AP configuration of magnetizations $\boldsymbol{M}_{Py}$ and $\boldsymbol{M}_{Co}$ for antiparallel arrangement at $H = 0$, and (b) of parallel arrangement at $H > H_S$. (c), (d) Mechanism of the SD transport corresponding to the AP and P configurations for the normal GMR effects. The mechanism points out a result of GMR with $J_{AP} < J_P$.

In the interpretation of the band-type model, the SD scattering mechanism is a "catch/reception" for inter-band spins. Both schemata point out that $J_{AP} < J_P$, which indicates a normal GMR effect. This representation is to repeat the SD scattering mechanism for the normal GMR effect observed in our low-T_a SV systems as mentioned above (e.g. Fig. 3(c, d)), as well as to compare more easily to the interpretation for the IMR mechanism presented below. Note that for the GMR effect, the MR nature has been attributed to contributions of spin-dependent scattering in *bulk* and at *interfaces*. Regarding the bulk scattering, impurities and failures in the lattice structure in the bulk of the FM layers caused the contribution. For the contribution of the interfaces scattering, a roughness of interfaces in the SVs should be the dominant parameter. A study to unambiguously separate these two contributions with negligible bulk defects has been done, for example, by Schad *et al*. [52]. The study pointed out that the magnitude of the GMR effect depends on both the vertical roughness amplitude and the step density. Moreover, a linear increase of the GMR with a product of the roughness amplitude and the step density has been found in this study. The interfacial roughness and steps will play a role in engineering the surface, such as controlling of spin scattering processes at interfaces. A model developed by Kumar *et al*. shows how the effect of interfacial spin-flip and momentum scattering on MR [53]. Especially, this result has also shown that a negative effect on MR due to spin-flip can be controlled by the interfacial resistivity. For the bulk scattering contribution, a study on dependence of MR on the bulk spin asymmetry scattering in FM layers with impurities has been done by Shiokawa *et al*. [54]. A theoretical study combining experimental analysis of the effects of both bulk and interface scattering on GMR can be found in Ref. [55].

The comments above on the bulk and interface SD scattering processes suggest the following assumptions, which are assigned to the SV system to describe the mechanism that leads to the IMR effect of the SVs annealed at High-Ta's. As known that, for an ordinary Py layer, $\alpha_{Py} > 1$ because of $N^{\downarrow}_{Py}(E_F) > N^{\uparrow}_{Py}(E_F)$ (e.g. see [50]), so $\rho^{\downarrow}_{Py} > \rho^{\uparrow}_{Py}$ due to $D^{\downarrow}_{Py} > D^{\uparrow}_{Py}$, as delegated by the band schema in Fig.6(a). This means the minority spin ($^{\downarrow}$) electrons are scattered more strongly than majority spin ($^{\uparrow}$) electrons. Whereas to get the IMR effect, it must be $\alpha_{Co} < 1$ in the Co layer. This can happen for several reasons. For example, an alloying or a diffusion process can take place at high temperatures in the layers of SV structure. When annealed at high temperature, diffuse processes back and forth are happening at once at the interfaces between the layers, so that thin layers of an alloy or a doped mixture/composite can be formed to insert, or all the SV's layers of the SVs will become alloyed or mixture. Such as, at the interface Py/Ag (Cu), an ultra-thin layer of alloy or mixture Py-Ag(Cu) can be inserted. Similarly, for an ultra-thin layer of alloy or mixture Co-Ag(Cu) can be formed and inserted into the interface Co/Ag(Cu). However, all these alloying or compositing layers do not cause a reversion in the spin density at the Fermi level to produce an IMR effect. In other words, even though the Py or Co layers are alloyed to become Py-Ag(Cu) and Co-Ag(Cu) alloying layers, their SSA coefficients remain so that $\alpha > 1$. Consequently, the normal GMR effect is still the dominant effect in such structures. Unless, one of the FM layers is alloyed or composited with atoms that belong to the group of transition metals with weak magnetic properties, such as V, Cr, and Mn. These can be confirmed by Refs. [7–17]. Therefore, it is perfectly reasonable to assume that $\alpha_{Py} > 1$. Completely similar to the above for the interface between the Co and MnNi layers when annealed at high temperatures, an alloying or compositing layer of Co-Mn or Co-Mn-Ni can be formed. As mentioned previously, Co alloy that contains Mn may be

responsible for $\alpha_{\text{'Co'}} < 1$. Vouille *et al*. have shown that $\alpha_{CoNi} > 1$ but $\alpha_{\text{CoMn}} < 1$ [13]. Hence, at high temperatures, the Co layer turns into a 'Co' layer which implies the fact that 'Co' is a Co-Mn-Ni alloy or composite leading to $\alpha_{\text{'}Co\text{'}} < 1$ is a completely realistic possibility. Therefore, for this 'Co' layer, $N^{\downarrow}_{\text{'}Co\text{'}}(E_F) < N^{\uparrow}_{\text{'}Co\text{'}}(E_F)$, and its arguments will be discussed later and presented below. Then $\rho^{\downarrow}_{\text{'Co'}} < \rho^{\uparrow}_{\text{'Co'}}$ due to $D^{\downarrow}_{\text{'Co'}} < D^{\uparrow}_{\text{'Co'}}$, which is depicted by a band schema as presented in Fig. 6(b). This implies that, the majority spin ($^{\uparrow}$) electrons are scattered more strongly than the minority spin ($^{\downarrow}$) electrons in the 'Co' layer.

Based on the above assumptions and comments as presented above, the mechanism of the IMR observed in the high-T_a annealed MnNi/Co/Ag(Cu)/Py SV systems could be imagined and interpreted as sketched in Fig.8. In this schema, $\boldsymbol{M}$ configurations corresponding with 4*s*-3*d* band structures in each layer are illustrated. In the case of $H = 0$, meaning $\boldsymbol{M}_{Py}$ and $\boldsymbol{M}_{Co}$ in the AP arrangement (Fig.8(a)), the minority spins ($^{\downarrow}$) are strongly scattered in the 'Co' layer due to $\alpha_{\text{'Co'}} < 1$ and again strongly scattered in the Py layer since $\alpha_{Py} > 1$. This indicates that the SV system gets a higher equivalent resistivity $\rho^{\downarrow}$ in the spins ($^{\downarrow}$) channel with the AP configuration. As a result, the transmission probability will be lower for the spin-($^{\downarrow}$) channel, like a blocking effect for the minority spin ($^{\downarrow}$) currents, as indicated by blue spins with their surface scatterings and trajectories between two scatterings being shown on the right in Fig. 8(a). For the majority spins ($^{\uparrow}$) in the AP configuration, a weak scattering in the both 'Co' and Py layers are dominated because of respectively to $\alpha_{\text{'Co'}} < 1$ and $\alpha_{Py} > 1$. This result creates a lower equivalent resistivity $\rho^{\uparrow}$ in the spins ($^{\uparrow}$) channel in the AP configuration, like a shunting effect for the majority spin ($^{\uparrow}$) currents, as indicated by red spins shown on the left in Fig. 8(a). Consequently, a total equivalent resistivity ρ_{AP} for both the spin channels of the 'Co'/Ag(Cu)/Py tri-layer in the AP configuration, ρ_{AP}, will become lower, or a total current density $\boldsymbol{J}_{AP}$ will be higher. In the context of spin transport of interband transitions for the AP configuration, as illustrated more clearly in Fig.8(c), the 'Co' spins ($^{\downarrow}$) (blue) are captured into the allowed Py spin ($^{\downarrow}$)-band so that almost no Py spins ($^{\downarrow}$) is transferred out the SV: $j^{\downarrow}_{Py} = 0$. Whereas, the 'Co' spins ($^{\uparrow}$) (red) cannot to be captured into the occupied Py spin ($^{\uparrow}$)-band, so that almost no Py spins ($^{\uparrow}$) to be transferred out the SV. This means $j^{\uparrow}_{Py}$ is close to zero, $j^{\uparrow}_{Py} \approx 0$. In this case, only the 'Co' spins ($^{\uparrow}$) are passed to create $J_{AP} = j^{\uparrow}_{\text{'Co'}} \neq 0$, as indicated by the bold solid trajectory on the left in Fig. 8(b) with a larger $N^{\uparrow}_{\text{'Co'}}(E_F)$. In the case of $H > H_S$, where a saturation magnetic field H_S is enough high so that $\boldsymbol{M}_{Py}$ and $\boldsymbol{M}_{\text{'Co'}}$ magnetizations are in complete parallel (P) arrangement (Fig. 8(c)). In this situation, the majority spins ($^{\uparrow}$) should have been strongly scattered to blocked the majority channel if the Co layer has $\alpha_{\text{'Co'}} > 1$ similar to $\alpha_{Py} > 1$ in the Py layer, to create the normal GMR effect (see Fig.7 (c,d)). However, here, these spins ($^{\uparrow}$) are scattered strongly only in the Py layer as usual, but become weaker in the 'Co' layer due to $\alpha_{\text{'Co'}} < 1$, as indicated by red trajectories shown on the left in Fig. 8(c). Such manner of scattering remains the same for the minority spins ($^{\downarrow}$), as indicated by blue trajectories shown on the right in Fig. 8(c). It means only a part of the 'Co' spins ($^{\uparrow}$) and ($^{\downarrow}$) were weakly scattered in the 'Co' layer due to $\alpha_{\text{'Co'}} < 1$, so that $j^{\uparrow}_{\text{'Co'}} \neq 0$ and $j^{\downarrow}_{\text{'Co'}} \neq 0$ to create a total current of $J_P = j^{\uparrow}_{\text{'Co'}} + j^{\downarrow}_{\text{'Co'}} \neq 0$, as represented by blue and red solid trajectories in Fig. 8(d). Even though these spins ($^{\uparrow}$) and ($^{\downarrow}$) are all scattered strongly in the Py layer, as represented by blue and red dashed trajectories in Fig.8(d), which implies that $j^{\uparrow}_{Py} = 0$ and $j^{\downarrow}_{Py} = 0$. The current

$j^{\uparrow}_{\text{'Co'}}$,is specified by all amount of $N^{\uparrow}_{\text{'Co'}}(E_F)$ in the P configuration, which is much smaller than $N^{\uparrow}_{\text{'Co'}}(E_F)$ in the AP configuration, because the Py spin ($^{\uparrow}$)-band has been completely occupied. While the current $j^{\downarrow}_{\text{'Co'}}$ is determined by a difference in DOS at the Fermi energy between the 'Co' spins ($^{\downarrow}$) and the Py spins ($^{\downarrow}$): $\delta N^{\downarrow}_{\text{'Co'}}(E_F) = N^{\downarrow}_{\text{'Co'}}(E_F) - N^{\downarrow}_{Py}(E_F)$. The total amounts of $N^{\uparrow}_{\text{'Co'}}(E_F)$ and $\delta N^{\downarrow}_{\text{'Co'}}(E_F)$ will determine the current $J_P \sim N^{\uparrow}_{\text{'Co'}}(E_F) + \delta N^{\downarrow}_{\text{'Co'}}(E_F)$. Finally, by comparing two spin transport processes in the AP and P configurations, it was noticed that $J_{AP} > J_P$, which implies the expected IMR effect.

For the above interpretation related to the so-called 'Co' layer, we need to emphasize here that this alleged layer is assumed to be newly formed from the origin Co layer by some factors after annealing at high-T_a's, to lead to $\alpha_{\text{'Co'}} < 1$. The problem is what causes the Co layer to become such 'Co' layer with $\alpha_{\text{'Co'}} < 1$? In fact, of the high-T_a annealed MnNi/Co/Ag(Cu)/Py SV

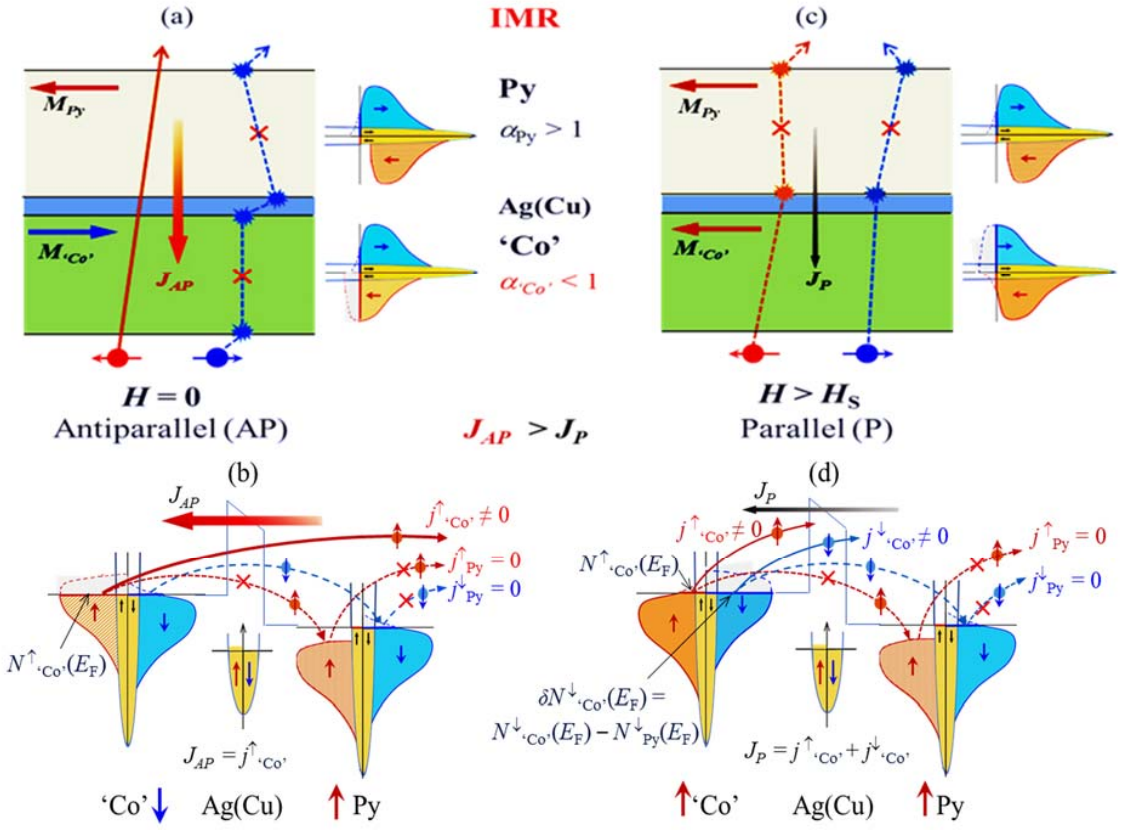

Fig. 8. (a), (c) Mechanism of the SD scattering for appearance of the IMR effect in the high-T_a annealed SVs with AP configuration at $H = 0$ and at $H > H_S$, respectively. (b), (d) Mechanism of the SD transport corresponding to the AP and P configurations for the IMR effects. The mechanism points out a result of IMR with $J_{AP} > J_P$, in opposition to normal GMR.

systems, it has been believed that there may be a process of diffusion taken place at the MnNi/Co interfaces by high temperatures, as mentioned above. If that is so, this process led to the formation of an alloyed or composited zone as a non-homogenous solid solution of Co, Ni and Mn and with unclear borders on both sides contacted with the Co and MnNi layers (see illustration in Fig.9(a)). The appearance of this alloying zone is equivalent to a buffer layer or sublayer inserted into the MnNi/Co interface. Component of a such buffer layer can be alleged being one of following possibilities: Mn:Ni:Co, Ni:Co, Mn:Co, or combined with a certain degree of mixing from all three types. Even both the MnNi and Co layers now can also become just a Mn:Ni:Co layer that has been called the 'Co' layer in the above paragraph. Here, confirming the presence of the Mn:Ni:Co alloy/compound layer and its microstructural features are necessary to make the arguments of the IMR effect more convincing. However, this requires a more careful and meticulous study, because it is tremendously difficult to confirm the composition of the alloy/compound by XRD measurements for a thin film layered relatively thinly and arranged in a rather small sample (see Fig.2). There are some other analytical techniques seemed more appropriate in this case. The analysis of chemical elements that are present at the Mn:Ni:Co alloy/compound zone can be performed using the X-ray photoelectron spectroscopy (XPS) or secondary ion mass spectrometry (SIMS) techniques. Nonetheless, such analysis should be done on another occasion. The symbol of Mn:Ni:Co or Ni:Co implies this is an unknown-component solid solution alloy or compound of the constituent atoms Mn, Ni and Co.

Coming back to the mechanism of the IMR effects related to the presentation of the buffer layer that is previously said. Although the nature of a common MR effect is attributed to contributions of spin-dependent scattering in bulk and at interfaces, previous studies have proved the IMR effect is mainly due to a bulk scattering process [9]. Nevertheless, it has been shown that, for SVs which possess one FM layer being a Co-alloy, the interfacial contribution produces only normal GMR effects at Co components below a certain moderate level and over a critical Co component threshold at very high Co contents while the bulk contribution produces the IMR effect only for the Co contents held an intermediate interval [56]. Meanwhile, another study on current-in-plane GMR effect of Fe/Cr/Au/Co system, where a very thin non-FM layer of Cr was inserted into Fe/Au interface, has demonstrated that the IMR effect is more dominant due to the spin-dependent interface scattering over than spin-dependent bulk scattering [57]. In Co/Ru/CoRu system [15], the negative GMR is attributed to the doping effect in CoRu alloy, which reduces the bulk spin-dependent scattering to a value smaller than the interface spin dependent scattering. For alloys containing only Fe, Co, and Ni, so-called equiatomic alloys, the majority-spin channel experiences negligible disorder scattering, thereby providing a short circuit [58]. On the other hand, ultrathin Mn:Co alloy with dilute Mn concentration had shown a dominant FM feature with a parallel coupling between Mn and Co magnetic moments [59]. Those imply the random solid solution alloys such as MnCo and CoNi show electronic properties of DOS and still maintain a status of $\alpha_{\mathrm{CoNi}} > 1$ like the origin Co layer. We suppose that it is burdensome to form an alleged layer being CoNi/MnCo solid solution alloy in the buffer zone.

Another possibility for the buffer zone is that it can be an Mn:Ni:Co solid solution alloy, while the remaining part in the bottle of the MnNi layer is just an incomplete AFM layer with dilute Mn concentration [see illustration in Fig. 9(a)]. The MnNi alloys are known as a typical AFM. However, this incomplete MnNi alloy in the thin-film form can be similar to the ultrathin Mn:Co alloy with dilute Mn concentration, which is implied to be a dominant FM feature. This may

be also one of the reasons leading to the weak EBC effect seen in the SV systems, as observed in hysteresis loops [see Fig.3(a),(b)]. Some studies have pointed out a trend of using d-block transition elements, such as V, Cr, Mn, for alloying of one of FM layers in SVs, which leads to IMR effect by conversion of the DOS at Fermi energy. For instance, in the FeV/Au/Co system, the IMR originates from the increase of the effective DOS at the Fermi level for majority spin electrons in Fe when it is alloyed with V. Following that there is an associated reversal of the spin scattering asymmetry factor from $\alpha > 1$ to $\alpha < 1$ in the $Fe_{1-x}V_x$ system [8]. For doping Mn, it has ever been found out that there is a transition from minority to majority spin transport in iron-manganese nitride $Fe_{4-x}Mn_xN$ films with increasing Mn concentration$x$ [60]. A recently published study on NiCoMn random alloys has pointed out that, for Mn containing equiatomic alloys, e.g. MnNiCo, both spin channels experience strong disorder scattering due to an electron filling effect [58]. Thus, from the above analysis one may be suggested that it is not important to explicitly form a subzone or a sublayer of a random alloy combined by Co, Ni, and Mn atoms, as a buffer zone/layer inserted between the Co and MnNi layers. But it can be considered that both layers should become a certain Mn:Ni:Co (MNC) random alloy zone after annealing at high-T_a's, as illustrated in Fig. 9(a), the so-called 'Co' layer in above paragraphs.

Based on data and analysis of Sai Mu *et al.* on electron scattering mechanisms in concentrated solid solution and high entropy alloys, such as NiFeCoCrMn alloys [60], the schema of the Fermi surface and energy scale of disorder scattering in NiCoMn alloys can be extracted to show a process of conversion in the DOS at the Fermi level during the doping Mn into NiCo. There is an increase in $N^{\uparrow}(E_F)$ in comparison with $N^{\downarrow}(E_F)$, as exhibited in Fig. 9 (b). From the above perceptions and based on the DOS calculated for NiCo alloys [61], we assume a schema of a DOS for the MnNiCo random alloys. This DOS schema is imagined as follows. Because the electrons redistribute due to doping Mn, the spin-up (majority) d-band is moved upward as sketched by a red dashed line in Fig. 9(c). This assumed DOS diagram assigned to the MnNiCo alloys can be reasonable and reliable, because studies on the influence of chemical disorder in concentrated solid solution alloys [61], such as MnNiCo, have shown a feature in DOS with a considerable increase in spin-up (majority) electrons. Especially, in the most recent study on hidden Mn magnetic-moment disorder and its influence on the physical properties of medium-entropy NiCoMn solid solution (random) alloys [62], one has been affirmed for this increase. Those results mean that the doped Mn atoms enhance $N^{\uparrow}(E_F)$, as sketched in Fig. 9(c). Mn situates in a distinctive position in the periodic table where the transformation between parallel and antiparallel coupling occurs. Hence, a slight change in the crystal structure of the films, relative to a true bulk structure, could lead to a massive change in the magnetic structure [59]. Gradually increasing the Mn concentration during a diffusion process due to the high temperature in the 'Co' zone (MNC) can take large-$N^{\uparrow,\downarrow}_{MNC}$ for both spin channels. This can lead to $\alpha_{MNC} \sim 1$ due to $N^{\uparrow}(E_F) \sim N^{\downarrow}(E_F)$ which cannot cause an occurrence of IMR. However, this is a random solid solution alloy that can fluctuate its Mn components, so that $\alpha_{MNC} < 1$ for causing an occurrence of IMR. In this case, the spin-dependent (SD) transport mechanism in the AP configuration for the SVs that present the 'Co' zone being an Mn:Ni:Co random alloy with $\alpha_{MNC} < 1$, similar to Fig. 8(b), should be represented as shown in Fig. 9(e). In this figure, the schematic DOS of the MnNiCo random alloy that shows in Fig. 9(c) was attached to the 'Co' zone; and a computational DOS of the NiFe alloys [50], as shown in Fig. 9(d), was applied to the Py layer of the SV systems. The schematic mechanism seems to express more clearly the IMR effect, where J_{AP} is contributed dominantly by the current $j^{\uparrow}_{\text{Co}'}$. The

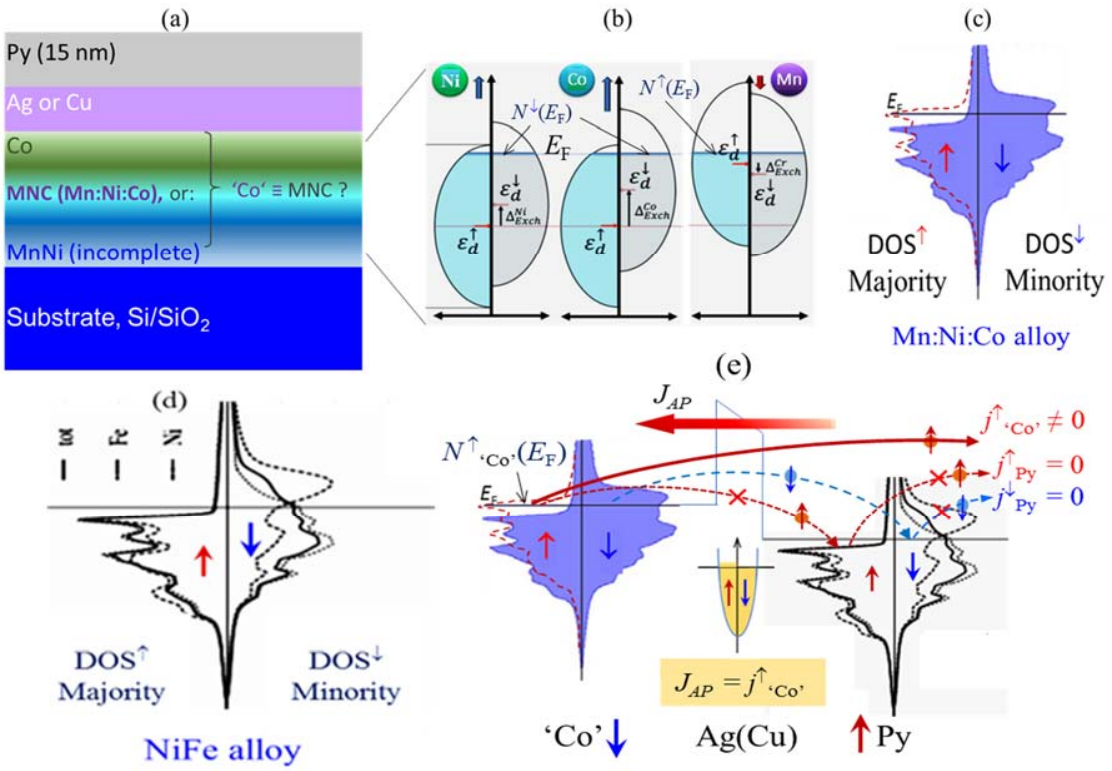

Fig. 9. (a) Illustration of cross-section structure of the MnNi/Co/Ag(Cu)/Py SVs with an alleged buffer of Mn:Ni:Co alloy, or an effective 'Co' zone of Mn:Ni:Co alloy. (b) Schematic illustration of shift in the DOS due to redistribution of electron spins in a Mn:Ni:Co alloy system (courtesy Ref. [58]). (c) The schematic DOS of a Mn:Ni:Co random alloy established (red dashed-line) based on the computational DOS of a NiCo alloy (gray filled-zone) (courtesy Ref. [61]) after being dopped by Mn. (d) The DOS of a fcc-Py alloy (black solid-line) (courtesy Ref. [50]). (e) Representation of Fig. 8(b) for the SD transport in the AP configuration of the structure shown in Fig. 9(a) with the 'Co' layer being a Mn:Ni:Co random alloy.

variation of the bulk asymmetric factor in the 'Co' layer with the random alloy composition can be also explained in terms of the variation of either the spin alignment of Co, Ni and Mn atoms, or the spin polarization of the 'Co' layer. This has happened similarly for Co and Gd atoms in a GdCo layer of system glass/Ta/NiO/Fe/Cu/$Gd_{1-x}Co_x$ SVs [58]. The total scattering spin asymmetry parameters in this case, $\alpha_{\text{'Co'}}$, or α_{MNC}, and α_{Py}, should be understood as comprising the bulk contribution of the respective FM layer ('Co') and contributions from the FM/NM interface ('Co'/Ag(Cu)) [57].

Another analysis for the IMR phenomenon can be based on the change in the sign of the spin-polarization of the DOSs (P_D) at the Fermi level E_F of the majority and minority spin electrons in two FM layers: $P_D = (D^{\downarrow} - D^{\uparrow})/(D^{\downarrow} + D^{\uparrow})$. A difference between the SD scattering

probabilities $D^{\downarrow(\uparrow)}$ in each FM layer is given by $\Delta = D^{\downarrow} - D^{\uparrow}$, and $P_D \sim \Delta$. Notice that P_D can receive extremely small values (≈ 0), > 0 or < 0. Under the normal status for both Py and 'Co' layers, $P_D > 0$ due to $N^{\downarrow}(E_F) > N^{\uparrow}(E_F)$. As known, the GMR ratio $\Delta R/R = (R_{AP} - R_P)/R_P \propto (D^{\downarrow}_{\text{'Co'}} - D^{\uparrow}_{\text{'Co'}})(D^{\downarrow}_{Py} - D^{\uparrow}_{Py})$ [8,9], where R_{AP} and R_P are resistivities of the SVs in AP and P configurations, respectively, thus $\Delta R/R \propto \Delta_{\text{'Co'}}\Delta_{Py}$, or $\Delta R/R \propto P_{D\text{'Co'}}P_{DPy}$. Therefore, the MR shows a normal GMR effect if the MR ratio $\Delta R/R > 0$ whenever the signs of $P_{D\text{'Co'}}$ and P_{DPy} are the same; and indicates an IMR effect if $\Delta R/R \propto P_{D\text{'Co'}}P_{DPy} < 0$ [57]. As seen here for the high-T_a annealed SV systems, since DOS of the Co layer has changed, and as previously assumed, the Co layer was renamed an alleged 'Co' layer so that $\alpha_{\text{'Co'}} < 1$ due to $D^{\downarrow}_{\text{'Co'}} < D^{\uparrow}_{\text{'Co'}}$, P_D in these SV systems should be $P_{D\text{'Co'}} < 0$ whereas $P_{DPy} > 0$. Thus, normal GMR effects, which have recorded in the as-deposited SVs and the low-T_a annealed SVs (T_a = 100˚C, 200˚C), or observed in some samples of SV1 and SV2 after annealing $T_a = 300$˚C and 400˚C, are because of either $P_{DCo} > 0$ and $P_{DPy} > 0$, or $P_{DCo} < 0$ and $P_{DPy} < 0$. While as, the IMR effects were observed only in some SVs that are annealed at the high-T_a's ($T_a = 300$˚C, 400˚C). In other words, the IMR effects can be essentially explained by the negative spin polarization of the Mn:Ni:Co random alloy in the 'Co' zone formed from alloying under high-$T_a$between the Co and MnNi layers. At the same time, it is also based on the negative spin scattering asymmetry at the 'Co'/Ag interface due to the difference of the spin arrangement structure according to the external magnetic field.

The nature of the NM layer, such as Ag or Cu, seems also to have a strong effect on the IMR effect in the High-T_a MnNi/Co/Ag(Cu)/Py SV systems. As seen in the case of Ag, see Fig. 5 (a)-(d) for SV1 and SV2, the IMR effect is observed only when SV1 annealed at 400˚C. A missing or quite faint IMR behavior in this SV1-SV2 system can supposedly attribute to a quite small 'Co'/Ag interface component contributed to the total scattering spin asymmetry parameter. Whereas, for the SV3-SV4 system, where the NM layers are Cu, see Fig.5 (e)-(h), with the IMR effect is observed in all SV3 and SV4, should be thought of very significant contribution into the total scattering parameter of the 'Co'/Cu interface component. The fact may be reasonable since the Co/Ag interfaces are supposed to be weaker SD scattering than the Co/Cu interfaces. In other words, the competition between scattering with $\alpha < 1$ and $\alpha > 1$ has led to both normal GMR and IMR in the SV1-SV2 system. This competitive situation is similar to the one that analyzed for (Fe/Cr/Fe)/Cu/Fe/Cu system [7], Fe/Cu/$Gd_{1-x}Co_x$ spin-valves [56], or Fe/Cr/Au/Co tri-layers [57]. The effect of the NM thickness on the IMR effect mainly focuses on the SV system with NM layer being Cu, SV3 and SV4 with t_{Cu} = 6 nm and 12 nm, respectively. Figs. 5(e)-(h) shows an unclear dependence in the IMR ratio on t_{Cu} increases. However, for the impact of annealing temperature, T_a = 300˚C, 400˚C, on the IMR effect of SV3 and SV4, the results show a marked increase in the IMR ratio as T_a increases. Generally, here, with limited data on $t_{Ag(Cu)}$ and T_a, it is difficult to see their influence on spin-dependent scattering in these high-T_a SVs.

IV. CONCLUSIONS

Magnetic transport in the MnNi/Co/Ag(Cu)/Py SV systems, characterized by the MR effects, has been investigated in various annealing temperatures ($T_a = 100$˚C $\div$500˚C) and Ag(Cu)-layer thicknesses (t_{Ag}, t_{Cu} = 6 nm and 12 nm). A change in the behavior of MR from a normal GMR to an IMR after annealing these SVs have been observed. Normal GMR behavior is observed for all the SV systems annealed at $T_a < 300$˚C for 30 minutes, while the IMR effect occurs only after

annealing these SVs at $T_a = 300^{\circ}$C and 400°C for 30 minutes. The IMR effect is occurred almost "no-rule" for the MnNi/Co/Ag/Py SV systems, while completely clear for the MnNi/Co/Cu/Py SV systems. Analysis and discussion in this work focus mainly on just the IMR effect of the SVs annealed at high-T_a's. An alloying process by diffusion that was attributed to taking place between the Co and MnNi layers, in which process the Co layer was diffused into the MnNi layer during annealing at high T_a, has been offered with the formation of a random alloying zone alleged to Mn:Ni:Co (MNC) solid solution. The IMR behavior has been explained primarily based on the idea that there is a tailoring of the density of states (DOS) from the formation of this MNC layer. The tailoring modifies the DOS in the alleged MNC layer and at the MNC/Ag interface so that to make a difference in their spin scattering asymmetry parameters α between the MNC and Py layers. The modifications lead to reverse $\alpha_{Co} > 1$ status for the origin Co layer into $\alpha_{MNC} < 1$ status for the alleged MNC layer, while keeping the $\alpha_{Py} > 1$ status for the Py layer. These results will contribute to a better understanding of the magnetic transport nature and of the potential of spin engineering for the SV systems, depending on the specific technological conditions, so that adjustments appropriate to the desired properties can be achieved.

ACKNOWLEDGMENTS

This work was supported by the project of Vietnam Ministry of Education and Training under Grant B2017-BKA-48.

REFERENCES

[1] B. Dieny, V. S. Speriosu, S. S. Parkin, B. A. Gurney, D. R. Wilhoit and D. Mauri, *Phys. Rev. B* **43** (1991) 1297.
[2] P. A. Grünberg, *Reviews of Modern Physics* **80** (2008) 1531.
[3] A. Fert, *Reviews of modern physics* **80** (2008) 1517.
[4] A. Guedes, R. Macedo, G. Jaramillo, S. Cardoso, P. P. Freitas and D. A. Horsley, *Sensors* **18** (2018) 790.
[5] L. Jogschies, D. Klaas, R. Kruppe, J. Rittinger, P. Taptimthong, A. Wienecke, L. Rissing and M. C. Wurz, *Sensors* **15** (2015) 28665.
[6] P. Pong, X. Liu and K. Lam, *Spintronic sensors, internet of things, and smart living*, Collaborative Conference on 3D & Materials Research, CC3DMR 2016, 2016.
[7] J.-M. George, L. G. Pereira, A. Barthélémy, F. Petroff, L. Steren, J.-L. Duvail, A. Fert, R. Loloee, P. Holody and P. A. Schroeder, *Phys. Rev. Lett.* **72** (1994) 408.
[8] J.-P. Renard, P. Bruno, R. Mégy, B. Bartenlian, P. Beauvillain, C. Chappert, C. Dupas, E. Kolb, M. Mulloy, P. Veillet et al., *Phys. Rev. B* **51** (1995) 12821.
[9] J.-P. Renard, P. Bruno, R. Mégy, B. Bartenlian, P. Beauvillain, C. Chappert, C. Dupas, E. Kolb, M. Mulloy, J. Prieur et al., *J. App. Phys.* **79** (1996) 5270.
[10] C. Bellouard, H. Rapp, B. George, S. Mangin, G. Marchal and J. Ousset, *Phys. Rev. B* **53** (1996) 5082.
[11] C. Vouille, A. Fert, A. Barthélémy, S.-Y. Hsu, R. Loloee and P. Schroeder, *J. Appl. Phys.* **81** (1997) 4573.
[12] J. Milano, A. Llois and L. Steren, *Phys. Rev. B* **66** (2002) 134405.
[13] C. Vouille, A. Barthélémy, F. E. Mpondo, A. Fert, P. Schroeder, S. Hsu, A. Reilly and R. Loloee, *Phys. Rev. B* **60** (1999) 6710.
[14] N. A. N. Thi, H. Y. N. Thi, H. Yi, S.-J. Joo and K.-H. Shin, *Phys. Status Solidi (a)* **204** (2007) 3954.
[15] K. Rahmouni, A. Dinia, D. Stoeffler, K. Ounadjela, H. Van den Berg and H. Rakoto, *Phys. Rev. B* **59** (1999) 9475.
[16] C. Marrows, F. Stanley and B. Hickey, *Applied Physics Letters* **75** (1999) 3847.
[17] A. Dinia, M. Guth, G. Schmerber and K. Ounadjela, *J. Appl. Phys.* **85** (1999) 4477.
[18] S. Maekawa and T. Shinjo, *Spin dependent transport in magnetic nanostructures*, CRC press, 2002.
[19] N. A. Tuan, N. T. Nhan, N. H. Ninh, T. V. Minh, N. Q. Huy and L. A. Tuan, *J. Korean Phys. Soc.* **72** (2018) 786.
[20] S. Parkin, *Annual Review of Materials Science* **25** (1995) 357.

[21] P. Bruno and C. Chappert, *Phys. Rev. Lett.* **67** (1991) 1602.
[22] W. Bennett, W. Schwarzacher and W. Egelhoff Jr, *Phys. Rev. Lett.* **65** (1990) 3169.
[23] S. Parkin, R. Bhadra and K. Roche, *Phys. Rev. Lett.* **66** (1991) 2152.
[24] C.-H. Chang, K.-P. Dou, Y.-C. Chen, T.-M. Hong and C.-C. Kaun, *Scientific reports* **5** (2015) 16844.
[25] A. Gayen, G. K. Prasad, K. Umadevi, J. A. Chelvane and P. Alagarsamy, *J. Magn. Magn. Mater.* **462** (2018) 29.
[26] C.-G. Lee, J.-G. Jung, V. Gornakov, R. D. McMichael, A. Chen and W. F. Egelhoff Jr, *J. Magn. Magn. Mater.* **272** (2004) 1887.
[27] C. Chappert and P. Bruno, *J. Appl. Phys.* **64** (1988) 5736.
[28] P. Bruno and J.-P. Renard, *Applied Physics A* **49** (1989) 499.
[29] P. Bruno, G. Bayreuther, P. Beauvillain, C. Chappert, G. Lugert, D. Renard, J. Renard and J. Seiden, *Journal of magnetism and magnetic materials* **93** (1991) 605.
[30] F. Rachford, M. Levy, R. Osgood Jr, A. Kumar and H. Bakhru, *J. Appl. Phys.* **87** (2000) 6253.
[31] T. McKinnon and E. Girt, *Applied Physics Letters* **113** (2018) 192407.
[32] P. Miltényi, M. Gierlings, M. Bamming, U. May, G. Güntherodt, J. Nogués, M. Gruyters, C. Leighton and I. K. Schuller, *Applied physics letters* **75** (1999) 2304.
[33] J. Sort, V. Langlais, S. Doppiu, B. Dieny, S. Suriñach, J. S. Muñoz, M. D. Baró, C. Laurent and J. Nogués, *Nanotechnology* **15** (2004) S211.
[34] H. Chang, C. Shen, F. Yuan, P. Pan, Y. Chien, C. Wang, L. Horng and S. Jian, *Thin Solid Films* **660** (2018) 834.
[35] T. Ambrose, R. Sommer and C. Chien, *Phys. Rev. B* **56** (1997) 83.
[36] H. Shi and D. Lederman, *Phys. Rev. B* **66** (2002) 094426.
[37] L. Sun, P. Searson and C. Chien, *Phys. Rev. B* **71** (2005) 012417.
[38] N. P. Thuy, N. A. Tuan et al., Proc. Inter. Conf. Eng. Phys., 2006, pp. 162–166.
[39] A. Berkowitz and K. Takano, *Journal of Magnetism and Magnetic materials* **200** (1999) 552.
[40] Y. Yüksel, *Physics Letters A* **382** (2018) 1298.
[41] S. Lee, J. Choi, S. Kim, J. Rhee and D. Hwang, *Journal of Magnetism and Magnetic Materials* **304** (2006) e91.
[42] S. Brück, J. Sort, V. Baltz, S. Surinach, J. S. Munoz, B. Dieny, M. D. Baró and J. Nogues, *Advanced Materials* **17** (2005) 2978.
[43] J.-V. Kim, R. Stamps, B. McGrath and R. Camley, *Phys. Rev. B* **61** (2000) 8888.
[44] M. D. Stiles, *Ch. 4: "interlayer exchange coupling" of ultrathin magnetic structures iii: Fundamentals of nanomagnetism*, eds. Bland, J Anthony C and Heinrich, Bretislav, Springer-Verlag Berlin Heidelberg, 2005.
[45] D. Bürgler, P. Grünberg, S. Demokritov and M. Johnson, *Handbook of Magnetic Materials* **13** (2001) 1.
[46] N. A. Tuan, L. Van Su, H. Q. Khanh, N. A. Tue and N. T. Luyen, *J. Korean Phys. Soc.* **72** (2018) 786.
[47] Z. Liu and S. Adenwalla, *J. Appl. Phys.* **93** (2003) 2091.
[48] N. F. Mott, *Proc. R. Soc.* **156** (1936) 368.
[49] A. Fert and I. Campbell, *J. de Phys. Colloques* (1971) C1.
[50] P. Yu, X. Jin, J. Kudrnovskỳ, D. Wang and P. Bruno, *Phys. Rev. B* **77** (2008) 054431.
[51] R. Lizárraga, F. Pan, L. Bergqvist, E. Holmström, Z. Gercsi and L. Vitos, *Scientific reports* **7** (2017) 1.
[52] R. Schad, P. Belien, G. Verbanck, K. Temst, V. Moshchalkov, Y. Bruynseraede, D. Bahr, J. Falta, J. Dekoster and G. Langouche, *Europhys. Lett.* **44** (1998) 379.
[53] S. B. Kumar, S. Tan and M. Jalil, *IEEE Trans. Magn.* **43** (2007) 2863.
[54] Y. Shiokawa, J. Jung, T. Otsuka and M. Sahashi, *J. Appl. Phys.* **118** (2015) 053909.
[55] B. Elsafi, F. Trigui and Z. Fakhfakh, *Compu. Mater. Sci.* **50** (2010) 800.
[56] D. Yang, B. You, X. Zhang, T. Gao, S. Zhou and J. Du, *Physical Review B* **74** (2006) 024411.
[57] M. Buchmeier, R. Schreiber, D. Bürgler and P. Grünberg, *Europhys. Lett.* **63** (2003) 874.
[58] S. Mu, G. D. Samolyuk, S. Wimmer, M. C. Troparevsky, S. N. Khan, S. Mankovsky, H. Ebert and G. M. Stocks, *npj Comp. Mater.* **5** (2019) 1.
[59] S. Banerjee et al., *J. Magn. Magn. Mater.* **198-199** (1999) 267.
[60] A. Anzai, T. Gushi, T. Komori, S. Honda, S. Isogami and T. Suemasu, *J. App. Phys.* **124** (2018) 123905.
[61] Y. Zhang, G. M. Stocks, K. Jin, C. Lu, H. Bei, B. C. Sales, L. Wang, L. K. Béland, R. E. Stoller, G. D. Samolyuk, M. Caro, A. Caro and W. J. Weber, *Nat. Commun.* **6** (2015) 8736.
[62] S. Mu, J. Yin, G. D. Samolyuk, S. Wimmer, Z. Pei, M. Eisenbach, S. Mankovsky, H. Ebert and G. M. Stocks, *Phys. Rev. Mater.* **3** (2019) 014411.